



PAPER

Spatially resolved spectroscopy of alkali metal vapour diffusing inside hollow-core photonic crystal fibres

OPEN ACCESS

RECEIVED
22 April 2022REVISED
7 October 2022ACCEPTED FOR PUBLICATION
26 October 2022PUBLISHED
10 November 2022

Original content from
this work may be used
under the terms of the
[Creative Commons
Attribution 4.0 licence](https://creativecommons.org/licenses/by/4.0/).

Any further distribution
of this work must
maintain attribution to
the author(s) and the
title of the work, journal
citation and DOI.

Daniel R Häupl^{1,2,*} , Daniel Weller³, Robert Löw³ and Nicolas Y Joly^{1,2} ¹ University of Erlangen-Nürnberg, Staudtstraße 7/B2, 91058 Erlangen, Germany² Max Planck Institute for the Science of Light, Staudtstraße 2, 91058 Erlangen, Germany³ 5th Physical Institute, University of Stuttgart, Pfaffenwaldring 57, 70569 Stuttgart, Germany

* Author to whom any correspondence should be addressed.

E-mail: daniel.haeupl@mpl.mpg.de**Keywords:** atomic physics, photonic crystal fibres, diffusion, spectroscopy

Abstract

We present a new type of compact and all-glass based vapour cell integrating hollow-core photonic crystal fibres. The absence of metals, as in a traditional vacuum chamber and the much more compact geometry allows for fast and homogeneous heating. As a consequence we can fill the fibres on much faster timescales, ranging from minutes to hours. Additionally the all-glass design ensures optical access along the fibre. This allows live monitoring of the diffusion of rubidium atoms inside the hollow-core by measuring the frequency-dependent fluorescence from the atoms. The atomic density is numerically retrieved using a five-level system of Bloch-equations.

1. Introduction

Hot atomic vapours are an active field of research and have great potential in the fields of quantum optics [1, 2] quantum communication [3, 4] or metrology [5, 6]. Optimal atom-light coupling in a vapour cell is limited by the diffraction limit of Gaussian beams. This can be overcome by confining light and atoms inside a hollow-core fibre. This led to many applications from nonlinear optics in noble gases [7], to chemistry [8], and three-photons spectroscopy of caesium vapour inside hollow-core photonic crystal fibres (hc-pcfs) [9]. While not using a fibre for confinement, attempts have been made for fully fibre-based spectroscopy setups [10]. Although previous works [9, 11, 12] showed the feasibility of filling hc-pcfs with hot vapours, the experimental setup was not optimal. The fibres were placed inside a conventional steel vacuum chamber filled with caesium. On the one hand, the large size of the steel chamber makes a homogeneous heating of the system not only technically challenging but prone to the creation of cold spots, reducing the vapour density at the position of the fibre. With this it takes accordingly longer until the entire fibre is in equilibrium with the background pressure and homogeneously filled. Uneven filling along the fibre length additionally creates severe static electric fields, troublesome for experiments with e.g. Rydberg atoms [13]. In this paper we present a new type of vapour cell that is entirely made out of glass. This includes a new way to mount the fibre inside the cell. These cells are not much larger than the fibre itself and offer an extended stem. Both regions are encapsulated by an appropriate two-zone oven with their respectively own heating circuits, preventing condensation in the main part by keeping the stem slightly cooler. Moreover, to allow full optical access from the side, the top of the oven consisting of two layers of glass windows. This way we can monitor the evolution of the atomic density distribution along the whole fibre length through the measurement of radially emitted fluorescence. From spatially resolved fluorescence we can deduce on what timescale the atoms diffuse into the fibre. Finally we modelled the frequency-dependent absorption of the light propagating inside the hollow-core using a five-level system to obtain a quantitative understanding of the diffusion process. At first, we present the concept of the gas-cell and how to hold the fibre properly. To study the dynamics of the filling process, we start in an equilibrium situation at a certain temperature and then suddenly raise or drop T and monitor how long it takes to undergo thermalisation.

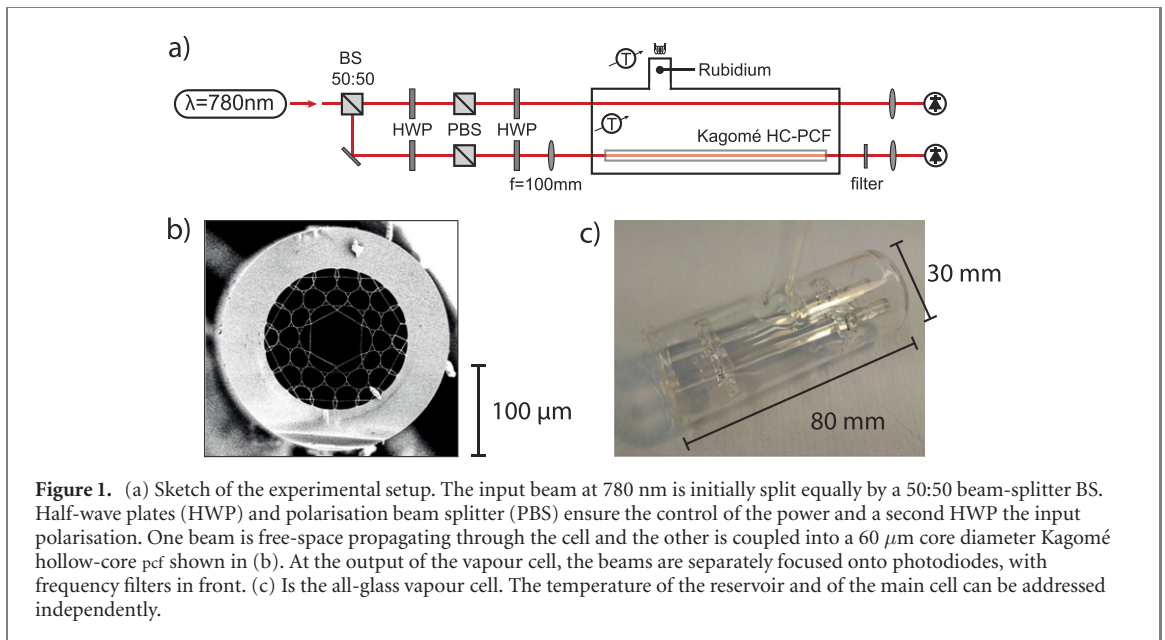
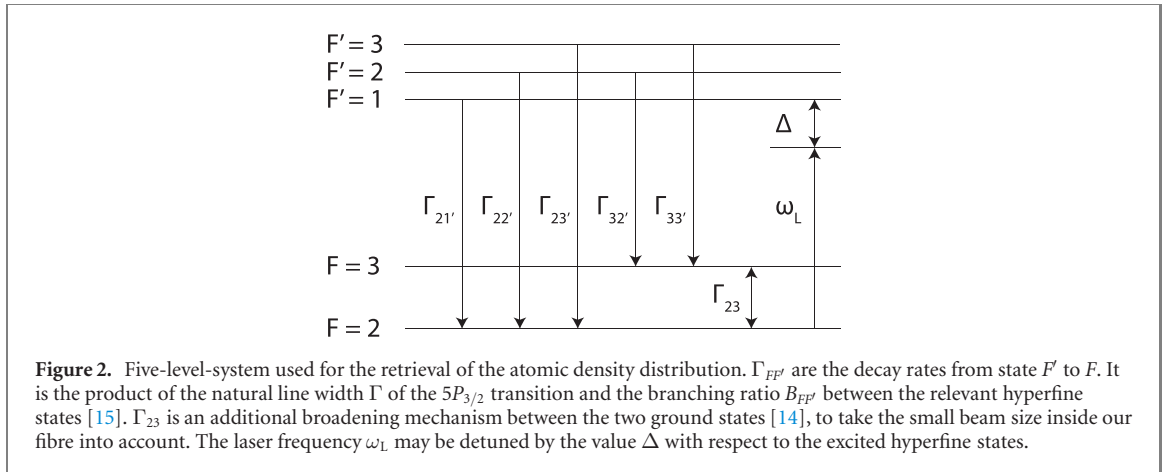


Figure 1. (a) Sketch of the experimental setup. The input beam at 780 nm is initially split equally by a 50:50 beam-splitter BS. Half-wave plates (HWP) and polarisation beam splitter (PBS) ensure the control of the power and a second HWP the input polarisation. One beam is free-space propagating through the cell and the other is coupled into a 60 μm core diameter Kagomé hollow-core pcf shown in (b). At the output of the vapour cell, the beams are separately focused onto photodiodes, with frequency filters in front. (c) Is the all-glass vapour cell. The temperature of the reservoir and of the main cell can be addressed independently.

2. Experimental setup

Optical setup. Our setup is depicted in figure 1(a). The pump comes from a linearly polarised Toptica DL-pro operated at 780 nm. The pump beam is split into two independent paths, both being sent to the gas-cell. The power of each beam line is controlled by a combination of half-wave plate and polarisation beam-splitter cube. We use a second half-wave plate to adjust the polarisation state at the entrance of the cell. One beam is coupled to a 60 μm core diameter Kagomé fibre using a lens with 100 mm focal distance. A scanning electron micrograph of the end face of the fibre is shown in figure 1(b). The fibre is 7.5 cm long, entirely made out of silica and was drawn at the fibre fabrication facilities at the Max-Planck Institute for the Science of Light. The second beam propagates freely through the gas-cell. At the output of the cell we monitor the transmitted power of the two beams with two photodiodes. Optical bandpass filters are inserted to prevent ambient light from perturbing the detected signal. The glass cell consist of a $\varnothing \times L = 30 \times 80 \text{ mm}^2$ tube made of borosilicate where two glass plates with cut-outs for the optical fibre are fixed to the inside walls. To ensure that the fibre is kept straight, we heat shrunk a 5 mm thick borosilicate tube around the bare optical fibre. The heat is provided via a small propane gas flame while rotating fibre and capillary using a lathe. The flame brushes the entire length of the capillary and fibre so as to collapse the capillary onto the silica fibre. Since borosilicate has a much lower softening temperature, the process does not affect the fine structure of the Kagomé fibre. The fibre-in-tube is not only more sturdy and can be hold in place with two glass supports, but due to the large thickness we are able to distinguish between fluorescence emitted in the hollow-core fibre and the background outside of it. This background light stems from leakage out of the fibre, non-perfect coupling and emitted fluorescence. Such a design gives access from the side over the complete length of the fibre, allowing side-scattering measurements. A secondary $\varnothing \times L = 5 \times 45 \text{ mm}^2$ tube is connected at 90° to the main cell and acts as the reservoir. Before filling the cell with the alkali metal, the cell is baked for 1 h at 330°C with a vacuum of better than 10^{-7} mbar. After pouring liquid alkali metal into the reservoir, the cell is sealed. In the current case we filled our cell with rubidium with its natural isotope distribution. The temperature of the reservoir and of the main cell can be addressed independently. The temperature of the reservoir is kept lower than that of the main cell. Therefore, not only is the atomic density given by the stem temperature but no Rb atoms will stick to the walls of the main cell. The diffusion of the rubidium atoms from the reservoir into the main cell is quite fast given the small dimensions and a steady state is achieved almost instantaneously. To accelerate the diffusion of the atoms into the fibre, we use elevated temperatures, increasing the overall atomic density. In principle we could work up to at least 300°C . However, at such temperatures neighbouring absorption lines start overlapping due to Doppler broadening. In this case our method to extract the atomic density fails. For this reason, we limit ourselves to temperatures up to 80°C .

Filling the vapour cell and the fibre. Ensuring a constant atomic density inside the fibre is of vital interest for experiments involving, e.g. Rydberg states. In order to monitor the filling process, we constantly measure the transmission spectra after our fibre and of a free-space beam through the glass cell itself, while scanning the pump wavelength through the complete D2 line of rubidium. We target the D2 transition



from ^{85}Rb $F = 2$ and model it using a Maxwell–Bloch equation approach, including the hyperfine states but neglecting the magnetic sublevels. In order to take into account the small beam size inside our fibre, we include transit time broadening [14] in our five-level-system (^{85}Rb ; $F = 2, 3$; $F' = 1, 2, 3$, figure 2). The evolution of the density matrix is governed by the Lindblad master equation [16, 17]

$$i\hbar\frac{\partial\rho}{\partial t} = [H, \rho] + i\hbar L_D(\rho), \quad (1)$$

with H the Hamiltonian of the system, ρ the density matrix and $L_D(\rho)$ the Lindblad operator

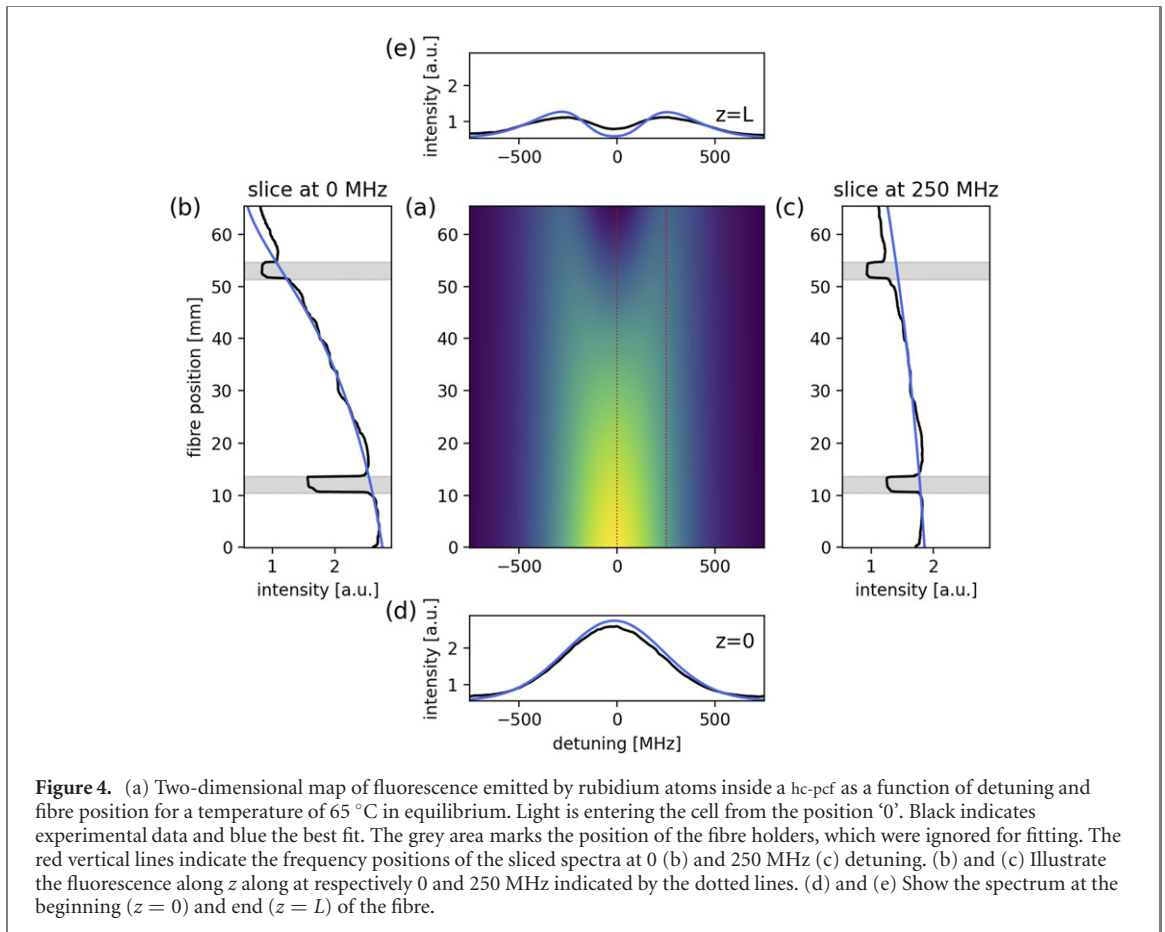
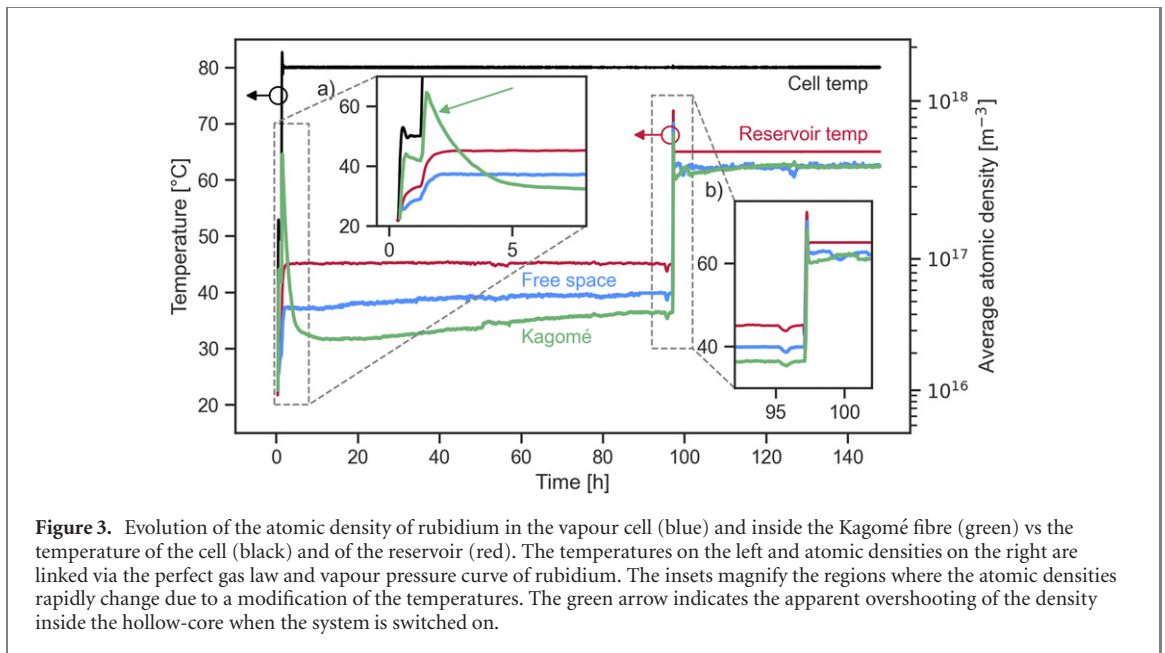
$$L_D(\rho) = \sum_{i,j} (\Gamma_{ji}\rho_{ij} - \Gamma_{ij}\rho_{ii})|i\rangle\langle i| - \frac{1}{2}\sum_{i\neq j} \left(\sum_k \Gamma_{ik} + \Gamma_{jk} \right) \rho_{ij}|i\rangle\langle j|. \quad (2)$$

There Γ_{ij} describes the decay from state $|j\rangle$ to $|i\rangle$ [15].

The measured spectrum corresponds to the steady state solution of equation (1), which yields the excited state fraction of the system. The off-diagonal elements of the density matrix lead to the complex valued electric susceptibility χ and thus the absorption coefficient. To ensure absolute calibration of the frequency-axis, part of the pump beam is guided through a Fabry–Perot interferometer. For intensities below the saturation intensity, we cross-checked our model to the ElecSus open source software [18] for which length, temperature, magnetic field, light polarization, etc can be adjusted. Note that ElecSus does not take power broadening into account, but it is implemented in our model. In our case, we work above saturation intensity and have to include this in our simulations. Beside the intensity, the temperature of the reservoir is the only fitting parameter, which yields the atomic density via the perfect gas law.

Figure 3 shows the evolution of the atomic density of rubidium in the vapour cell and inside the Kagomé fibre for different temperatures of the cell and of the reservoir. Moreover, the cell was not cured prior this experiment, but had already been heated at $\approx 50^\circ\text{C}$ for 20 h. At all times we made sure that the temperature of the reservoir remains lower than that of the main cell. In the initial stage (figure 3(a)) the vapour cell is heated from room temperature to 80°C and left there for 96 h. During that time, the reservoir is left at ambient temperature and only heats up due to the conduction of the oven, reaching 45°C . As shown in figure 3(a), as the oven is switched on, the density of atoms in the main cell rapidly increases (blue line). Surprisingly, the estimation of the density of rubidium retrieved from the spectrum at the output of the fibre overshoots the value that is expected for such a temperature of the reservoir. We reproducibly observe this whenever we turn on the system. One possible reason being, that even at room temperature rubidium metal diffused into the fibre and stuck to the core wall. When we then increase the temperature, those atoms might desorb and after roughly 5 h the system has relaxed. Afterwards the density inside the fibre increased with a time constant of 45 h. In a second step—after 96 h—we increased the reservoir temperature to 65°C , while keeping the cell temperature at 80°C . From the free-space measurement (blue line) we see that the cell follows almost instantaneously the change of temperature of the reservoir and reacts within less than $1/2$ h. We can therefore consider that it is fully cured at that time.

In case of our Kagomé fibre (green line), we also observe this rapid change, but the atomic density reached an equilibrium after ~ 24 h, with a timescale of 9.4 h for the diffusion process. This should be compared to the previous experiment using a $60\ \mu\text{m}$ core diameter Kagomé fibre. At that time the filling process lasted >20 days [19].



To even better understand the diffusion in/out of the fibre for an increase/decrease of the gas pressure in the main cell, we additionally look at the radial fluorescence along the fibre. In a simple picture, the atomic density should be proportional to the emitted fluorescence. As a proof of principle, we decrease the temperature of the cell, corresponding to a reduction of the atomic density in the surrounding glass cell and causing a density gradient between the fibre and the cell. We chose a temperature decrease, giving us more time for a careful study of the system dynamics. Specifically, we decreased the reservoir temperature from 65 to 45 °C while keeping the cell temperature at 80 °C and monitored the diffusion process over 100 h. While

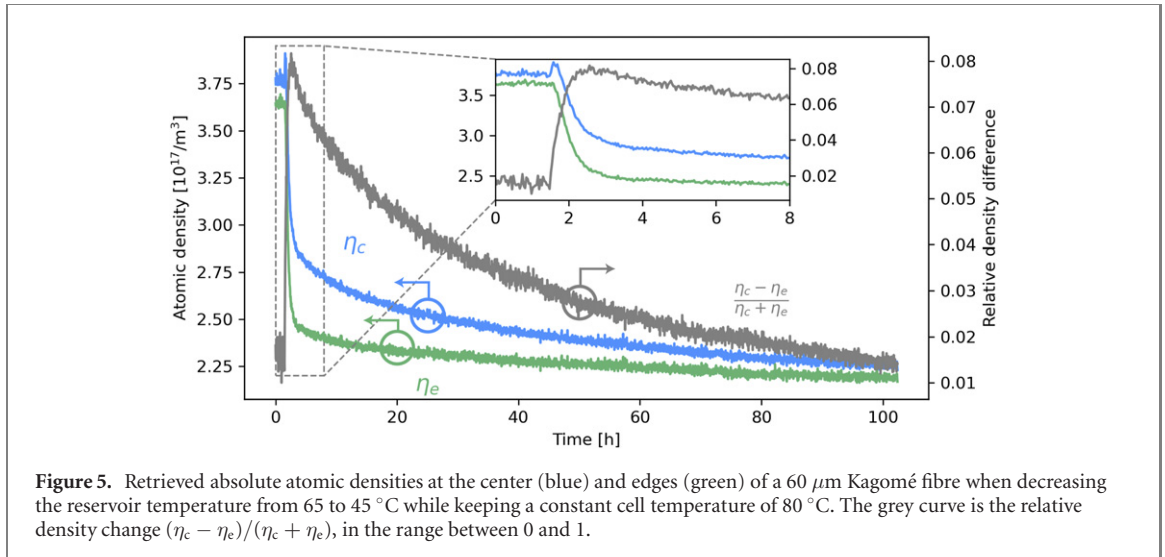


Figure 5. Retrieved absolute atomic densities at the center (blue) and edges (green) of a 60 μm Kagomé fibre when decreasing the reservoir temperature from 65 to 45 $^{\circ}\text{C}$ while keeping a constant cell temperature of 80 $^{\circ}\text{C}$. The grey curve is the relative density change $(\eta_c - \eta_e)/(\eta_c + \eta_e)$, in the range between 0 and 1.

the rubidium diffuses out of the fibre, we take a series of pictures using a 14 bit ccd camera mounted above our glass cell. To obtain a full spectrum we scan the laser over the $D2 F = 2$ transition of ^{85}Rb and image the glass cell every 17.5 MHz of laser detuning. The input polarisation was chosen so that maximum intensity was recorded by the CCD camera. The complete scan takes 25 s, which is well below the diffusion timescale that we measured previously (figure 3). Each image is transversally integrated within the region of interest to obtain a one-dimensional intensity distribution along the propagation. By stacking these 160 pictures for all recorded frequencies, we obtain a two-dimensional map of the emitted fluorescence as a function of detuning and fibre position as shown in figure 4. The resolution of these maps is around 160×870 (detuning \times length), depending on the acquisition speed of the camera. On figures 4(b) and (c) the black lines represent the raw experimental data for two specific frequencies and the blue lines our model.

We extract the evolution of the density inside the fibre for a specific detuning Δ of the pump using the Beer–Lambert law. This is done in an iterative way along the whole length of the fibre, assuming an initial intensity $I(z = 0)$ and an atomic density $\eta(z = 0)$. As the light propagates the intensity decreases according to

$$\frac{dI}{dz} = \frac{4\pi}{\lambda} \text{Im} \left\{ \sqrt{1 + \chi[\eta(z), I(z), \Delta]} \right\} I(z), \quad (3)$$

where the susceptibility χ depends on the light intensity $I(z)$ and is directly proportional to the atomic density $\eta(z)$. This is directly linked with the optical density OD through

$$\text{OD}(z) = -\frac{2\pi}{\lambda} z \text{Im} \left\{ \sqrt{1 + \chi[\eta(z), I(z), \Delta]} \right\}. \quad (4)$$

As we lower the temperature of the reservoir, the density of atoms inside the cell will decrease, yielding a symmetric diffusion of atoms out of both ends of the fibre. For simplicity, we assume that the atomic density distribution follows

$$\eta(z) = (\eta_c - \eta_e) \cdot \left\{ 1 - \tanh^2 \left[\sigma \cdot \left(z - \frac{L}{2} \right) \right] \right\} + \eta_e, \quad (5)$$

with L the fibre length, η_e and η_c respectively the atomic density at both ends and at the center of the fibre. σ is chosen so that $\eta(0) = \eta(L)$ is within 1% of η_e . This approximately corresponds to a factor of $\sigma = \frac{6}{L}$. The measured fluorescence (black lines in figures 4(b) and (c) is directly linked with the atomic density and the excited state fraction. Combining the steady state solution of (1) with an assumed distribution of (5), we calculate η_e and η_c . As shown on figures 4(b) and (c) the calculated fluorescence curves (blue lines) along the fibre length agree very well with our experimental data. Figures 4(d) and (e) show the fluorescence spectra at the beginning and the end of the fibre at a given time t . As the diffusion process takes place, we record a series of these maps which are processed the same way. Figure 5 shows the temporal evolution of the absolute atomic density at the end (η_e) and in the center (η_c) of the fibre. It is clear that the atomic density at the edge rapidly decreases (green curve) following the change in the cell. The change in the center (blue curve) is much slower, because the rubidium atoms need to diffuse out of the fibre. Like the

transmission measurement (figure 3), the fluorescence measurement shows that the atomic density rapidly changes as soon as the reservoir temperature is modified (figure 5). After this abrupt drop the evolution of the atomic density is much slower, with timescales of $\tau_c = 36$ h and $\tau_e = 45$ h, when fitting with a double exponential decay of the form

$$\eta(t) = a e^{-t/\tau_1} + b e^{-t/\tau_2} + c. \quad (6)$$

Here τ_c respectively τ_e is the larger of the two lifetimes τ_1/τ_2 , corresponding to the slower diffusion timescale of the system. To conclude, we presented here an all-glass assembly integrating alkali vapours with a hollow-core photonic crystal fibre. Its small dimensions and homogeneous temperature permit a rapid modification of the atomic density in a controlled way. Additionally, the all-glass design allows to perform easily accessible measurements from the side. Measuring the fluorescence of the rubidium allows observing in real-time and spatially resolved the diffusion of the atoms out of the fibre when changing the atomic density inside the vapour cell. Both transmission and fluorescence measurements confirm that the atomic density inside the fibre has reached an equilibrium only after a few days. This drastically contrasts with previous experiments, where hollow-core fibres were filled with hot caesium metal in bulky metal based vacuum chambers [13]. We believe that such a cell makes an attractive tool for atomic spectroscopy, Rydberg physics and non-linear optics. Its small size makes this type of cells more transportable and integration in an spectroscopy setup much easier. In a next step it would be interesting to have an all fibre based setup to avoid free beam coupling to the fibre [10].

Acknowledgments

This project is supported by the DFG (JO 1090/4-1, LO 1657/6-1 & RU 1426/1-1) as part of the SPP 1929 ‘Giant Interactions in Rydberg Systems (GiRyd)’. We also thank SAOT for financial support.

Data availability statement

The data that support the findings of this study are available upon reasonable request from the authors.

ORCID iDs

Daniel R Häupl  <https://orcid.org/0000-0002-2446-4307>

Nicolas Y Joly  <https://orcid.org/0000-0001-9654-4624>

References

- [1] Caltzidis I *et al* 2021 Atomic Faraday beam splitter for light generated from pump-degenerate four-wave mixing in a hollow-core photonic crystal fiber *Phys. Rev. A* **103** 043501
- [2] McCormick C F, Boyer V, Arimondo E and Lett P D 2007 Strong relative intensity squeezing by four-wave mixing in rubidium vapor *Opt. Lett.* **32** 178–80
- [3] Finkelstein R *et al* 2018 Fast, noise-free memory for photon synchronization at room temperature *Sci. Adv.* **4** eaap8598
- [4] Kaczmarek K T *et al* 2018 High-speed noise-free optical quantum memory *Phys. Rev. A* **97** 042316
- [5] Budker D and Romalis M 2007 Optical magnetometry *Nat. Phys.* **3** 227–34
- [6] Meyer D H, Kunz P D and Cox K C 2021 Waveguide-coupled Rydberg spectrum analyzer from 0 to 20 GHz *Phys. Rev. Appl.* **15** 014053
- [7] Travers J C, Chang W, Nold J, Joly N Y and St. Russell P J 2011 Ultrafast nonlinear optics in gas-filled hollow-core photonic crystal fibers [invited] *J. Opt. Soc. Am. B* **28** A11–26
- [8] Cubillas A M, Unterkofler S, Euser T G, Etzold B J M, Jones A C, Sadler P J, Wasserscheid P and Russell P S J 2013 Photonic crystal fibres for chemical sensing and photochemistry *Chem. Soc. Rev.* **42** 8629–48
- [9] Epple G *et al* 2014 Rydberg atoms in hollow-core photonic crystal fibres *Nat. Commun.* **5** 4132
- [10] Gutekunst J, Weller D, Kübler H, Negel J-P, Ahmed M A, Graf T and Löw R 2017 Fiber-integrated spectroscopy device for hot alkali vapor *Appl. Opt.* **56** 5898
- [11] Ghosh S *et al* 2006 Low-light-level optical Interactions with rubidium vapor in a photonic band-gap fiber *Phys. Rev. Lett.* **97** 023603
- [12] Light P S, Benabid F, Couny F, Maric M and Luiten A N 2007 Electromagnetically induced transparency in Rb-filled coated hollow-core photonic crystal fiber *Opt. Lett.* **32** 1323–5
- [13] Epple G, Joly N Y, Euser T G, St. Russell P J and Löw R 2017 Effect of stray fields on Rydberg states in hollow-core PCF probed by higher-order modes *Opt. Lett.* **42** 3271–4
- [14] Urvoy A, Carr C, Ritter R, Adams C S, Weatherill K J and Löw R 2013 Optical coherences and wavelength mismatch in ladder systems *J. Phys. B: At. Mol. Opt. Phys.* **46** 245001
- [15] Masalov A V and Minogin V G 2014 Spontaneous decay rates of the hyperfine structure atomic states into an optical nanofiber *J. Exp. Theor. Phys.* **118** 714–22
- [16] Allen L and Eberly J H 1987 *Optical Resonance and Two-Level Atoms* (New York: Dover)

- [17] Breuer H-P and Petruccione F 2007 *The Theory of Open Quantum Systems* (Oxford: Oxford University Press)
- [18] Zentile M A, Keaveney J, Weller L, Whiting D J, Adams C S and Hughes I G 2015 ElecSus: a program to calculate the electric susceptibility of an atomic ensemble *Comput. Phys. Commun.* **189** 162–74
- [19] Epple G 2017 Spectroscopy of Rydberg atoms in hollow-core photonic crystal fibers *PhD Thesis* Friedrich-Alexander-Universität Erlangen-Nürnberg